Supplementary Figure 1

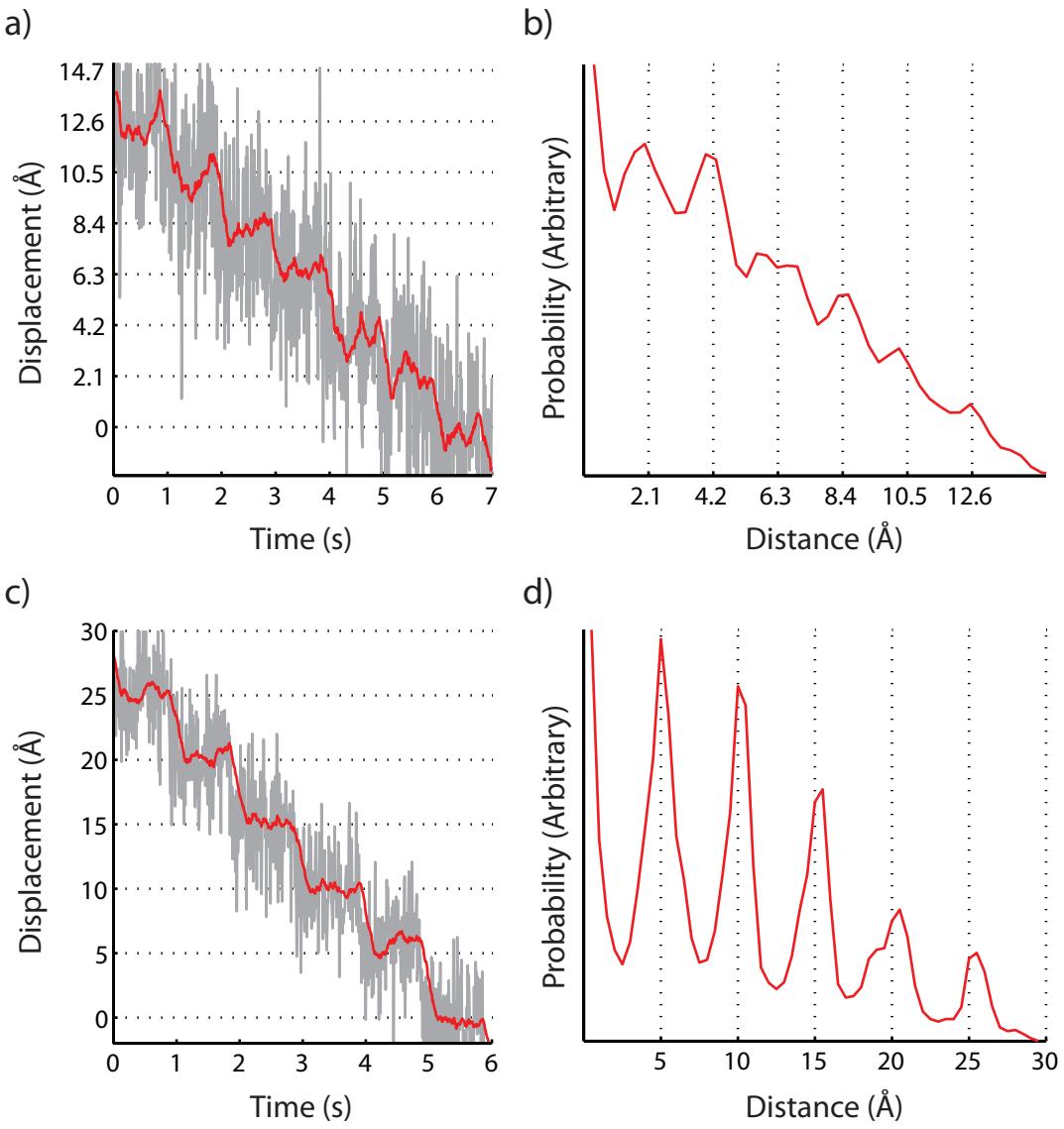

Supplementary Figure 1. Optical trap detection resolution demonstration. Steps are introduced into trapped bead positions (tethered by 3.4-kbp dsDNA) by stepping the position of one trap every 1 second simulating steps in tether extension that might be seen in an experiment (e.g., motor protein stepping). The measured difference in the two bead positions (differential measurement) is plotted at 120 Hz (gray, boxcar averaged from 67 kHz raw acquisition rate) and 4 Hz (red, running average of gray curve) bandwidths. (b) and (d) pairwise distributions of 4 Hz stepping data from (a) and (c) respectively. (a) and (b) 9.1 ± 0.1 pN tether tension, trap stepped in 3.4 Å (1 base pair) increments results in clear 2.5 Å steps in bead displacement. (c) and (d) 9.7 ± 0.1 pN tether tension, larger trap step increment of 8.0 Å results in even clearer 5.0 Å steps in bead displacement. Observed bead displacements are less than trap displacements due to tether compliance.

Supplementary Figure 2

a)

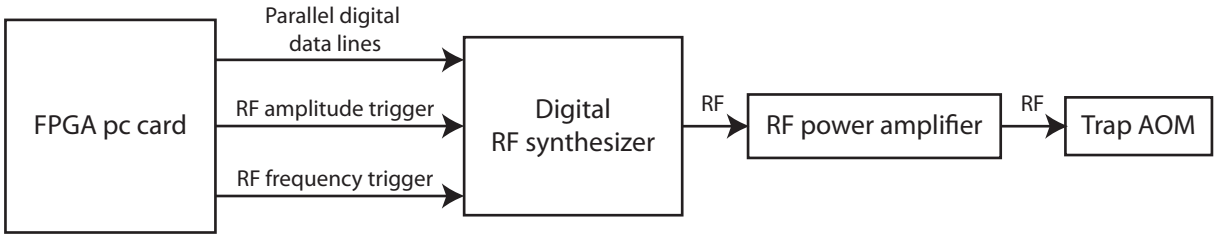

b)

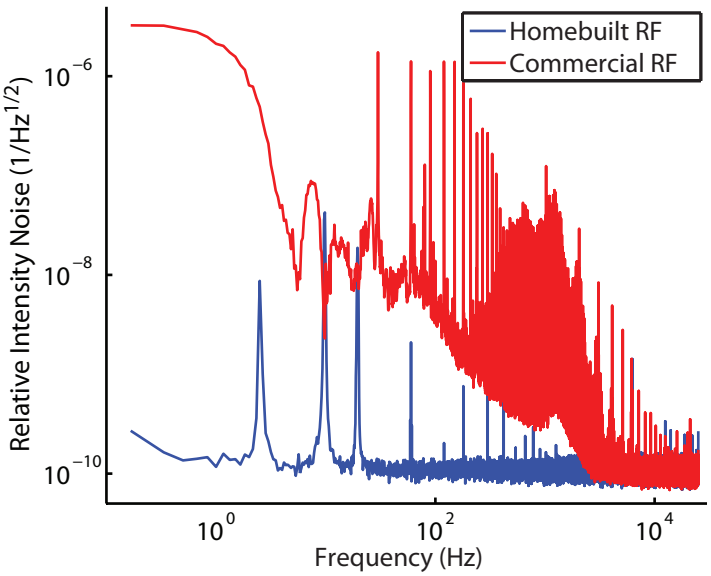

Supplementary Figure 2. Homebuilt RF electronics improves optical trap stability. (a) Diagram of components of RF synthesis electronics and their connectivity (see Methods for details). (b) Trap intensity noise with acousto-optic device driven by our homebuilt RF electronics (blue) vs. device manufacturer RF electronics (red, IntraAction DVE-120 pc card).

Supplementary Figure 3

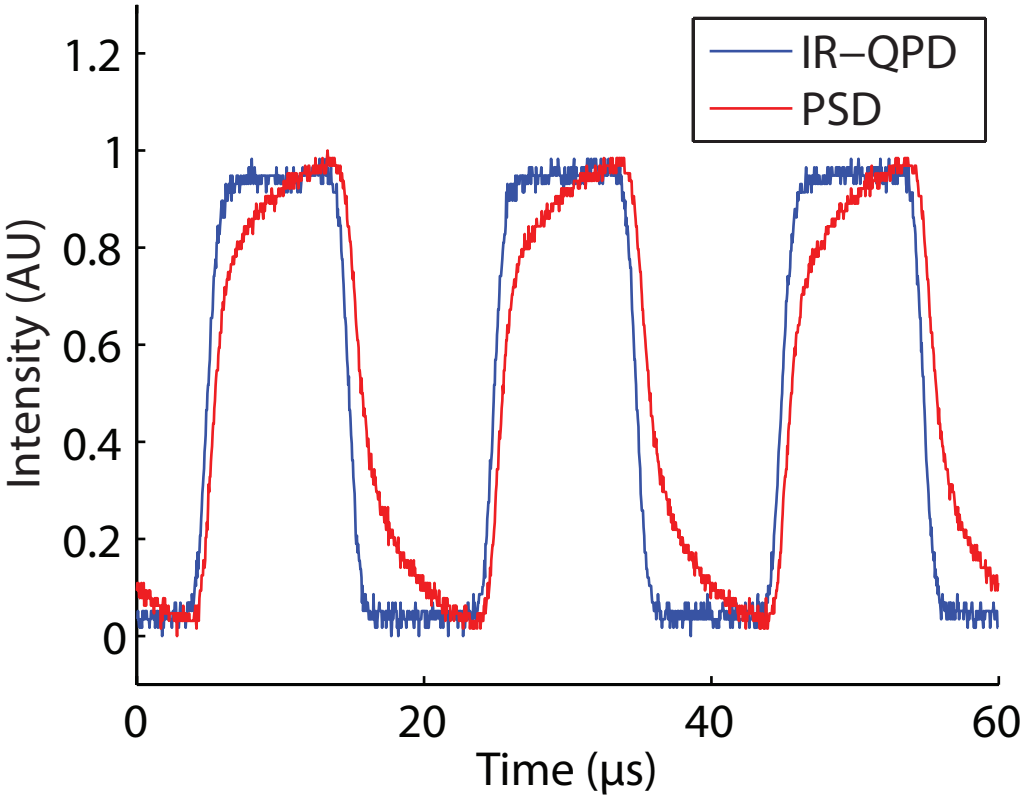

Supplementary Figure 3. A fast bead position detector is used for high-speed timesharing/interlacing of optical traps. Optical trap intensity during 50-kHz interlacing measured simultaneously by IR-enhanced QPD (blue, fast response) and standard PSD (red, slow response) photodetectors. The IR-enhanced QPD is operated at 50 V reverse bias. Position measurements show the same speed enhancement.

Supplementary Figure 4

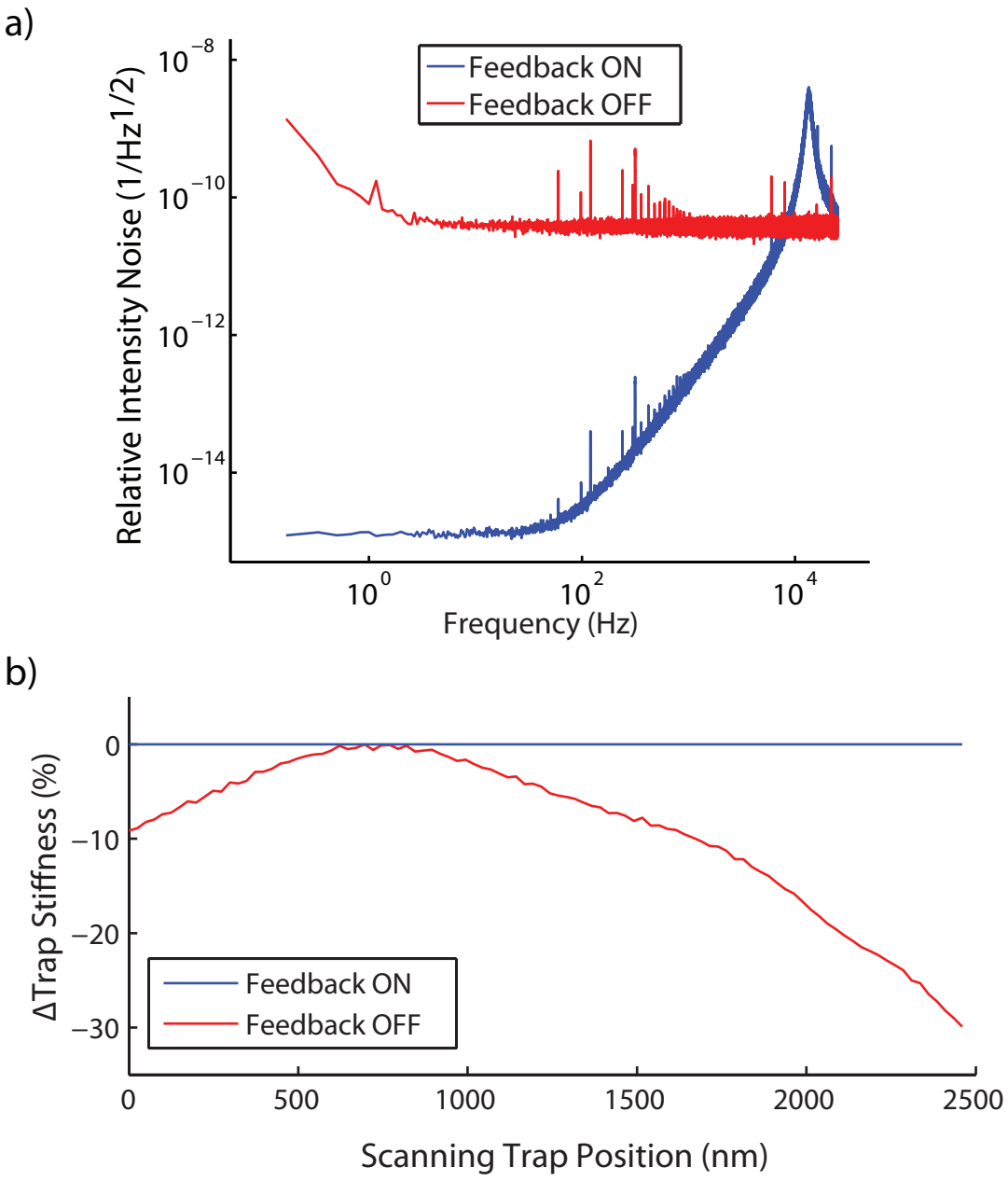

Supplementary Figure 4. Feedback on optical trap intensity greatly reduces optical trap intensity noise and stabilizes trap stiffness while scanning the trap position. (a) Trap intensity noise with feedback on (blue) or off (red). (b) Change in trap stiffness as AOM scans the trap position with feedback on (blue) or off (red).

Supplementary Figure 5

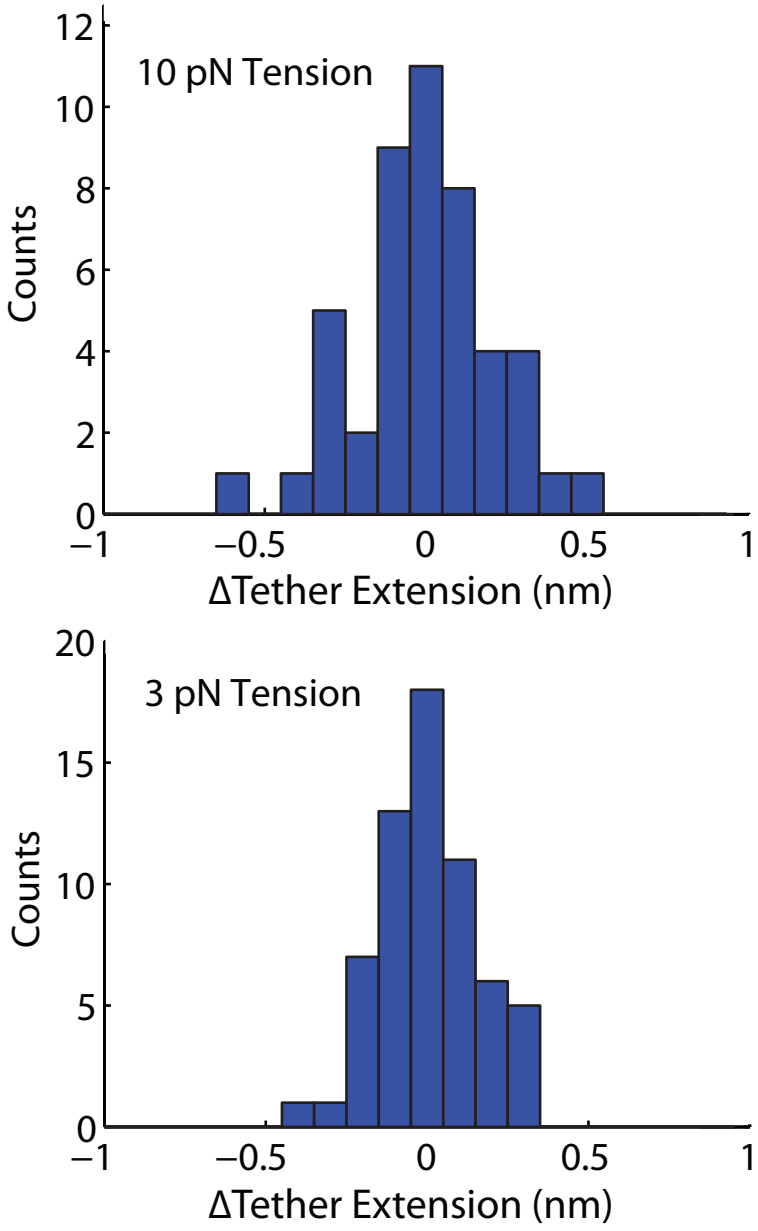

Supplementary Figure 5. Control measurements showing the change in tether extension measured without a probe strand binding to the tether. The distributions are composed of individual measurements of the difference in tether extension averaged for 3 s after and before a time point chosen at random (rather than by using the stepwise fluorescence increase-decrease as in the case of probe strand binding and unbinding) for tether tensions of 10 pN (upper panel) and 3 pN (lower panel). These distributions are otherwise derived from exactly the same experiments and using the exact same data analysis routine as used to produce the actual binding and unbinding distributions in Fig. 4c (10 pN) and f (3 pN). For both tensions, the distributions are centered at zero extension change [as expected, 0.00 ± 0.03 nm and 0.01 ± 0.02 nm for 10 pN and 3 pN respectively (errors are s.e.m.)] and the widths of the distributions match the widths of the actual binding and unbinding extension change distributions at corresponding tensions (standard deviations of 10 pN and 3 pN distributions are 0.21 nm and 0.15 nm respectively). This means that the widths of the binding and unbinding extension change distributions are not primarily due to actual variation of tether extension change upon binding/unbinding, but are rather indicative of the intrinsic noise of tether-beads-traps system.

Supplementary Figure 6

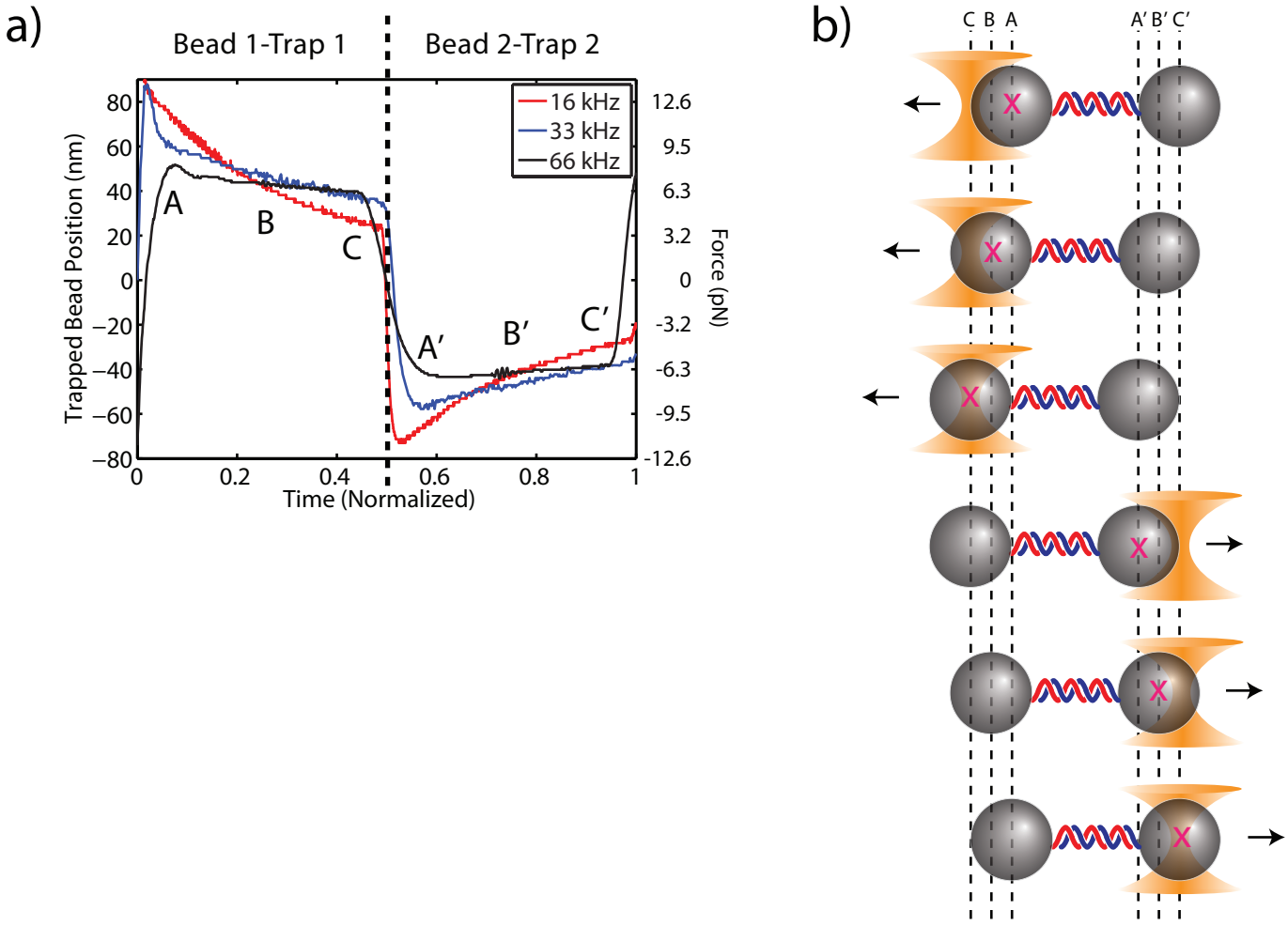

Supplementary Figure 6. Effect of timesharing-interlacing method on trapped bead positions and resultant data acquisition considerations. (a) High-speed measurements of trapped beads' positions during one timesharing/interlacing cycle are shown for three different timesharing/interlacing rates. The data are measured by QPD1 as usual but are recorded by a storage oscilloscope (2-GHz sampling rate) instead of the usual FPGA-based DAQ card analog inputs (only 200-kHz max sampling rate). The data time scales are normalized to the timesharing/interlacing cycle duration. Only the first two thirds of the timesharing/interlacing cycle are shown (first and second half of the plot), where first trap 1 is ON measuring the position of bead 1 and then trap 2 is ON measuring the position of bead 2. The final third of timesharing/interlacing cycle when both traps are OFF and fluorescence data is acquired is not shown. Bead positions are labeled with letters. Faster timesharing/interlacing speed minimizes bead oscillations. Bead oscillations are illustrated in (b). The letters labeling the positions of the beads in the drawing (b) correspond to the labeled positions in the measurement (a). Data acquired in the middle of the bead oscillation period (the middle of the corresponding trap ON period), at time points B and B' will give a correct measure of the DNA tether length, whereas data measured at time points A and A' or C and C' will respectively under- and overestimate DNA tether length.

Supplementary Figure 7

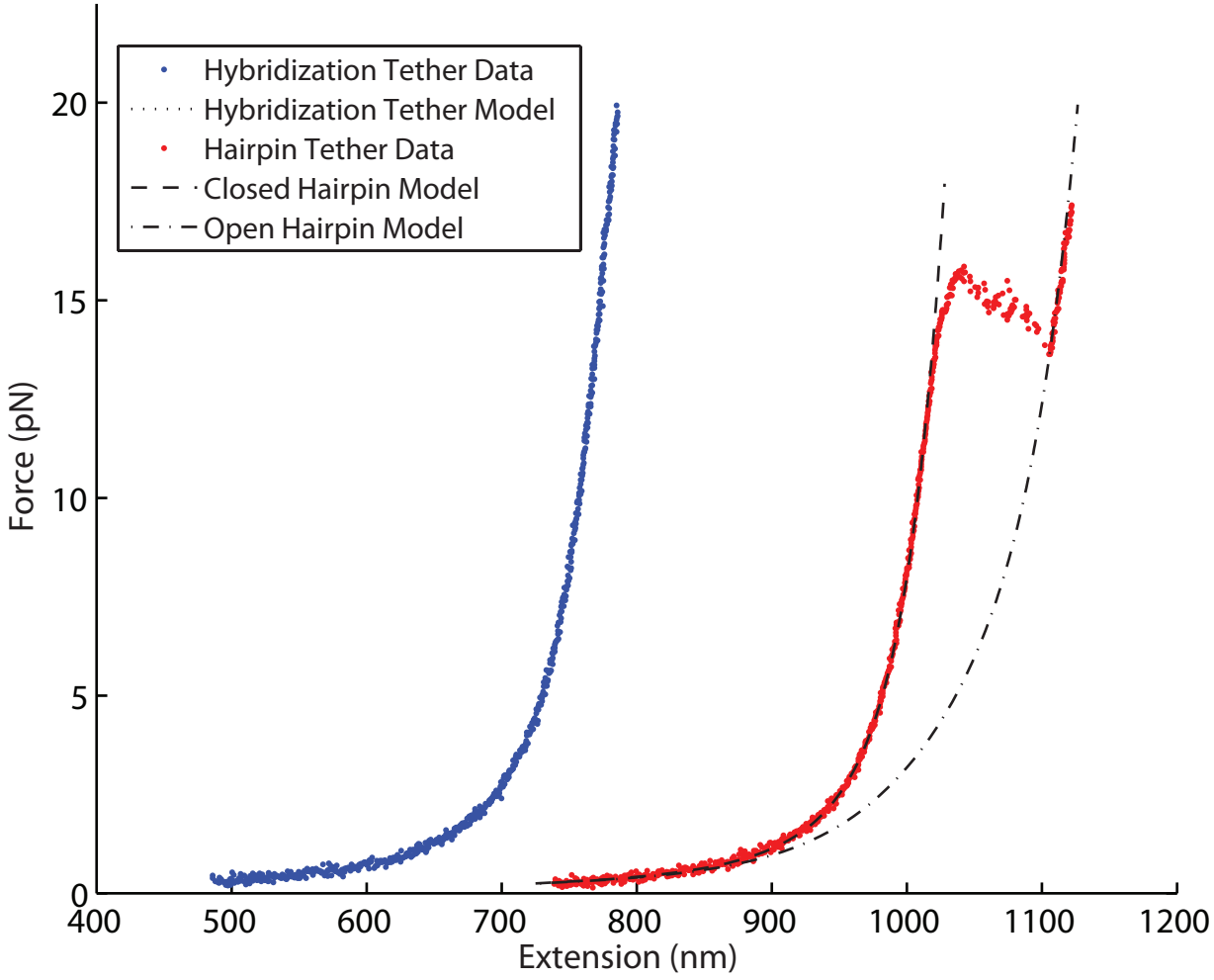

Supplementary Figure 7. Force-extension curves of two different DNA tether constructs demonstrating instrument performance. In red: example force-extension curve of a 3.05-kbp long dsDNA construct containing an 89-bp long hairpin. The dashed and dashed-dotted lines are polymer models of the DNA construct with the hairpin either closed or open respectively (see Methods). The measured hairpin opening force (15.8 pN) agrees well with independent measurements (15.9 pN) made by a second, well-calibrated instrument [Landry, M.P., McCall, P.M., Qi, Z., & Chemla, Y.R. Characterization of photoactivated singlet oxygen damage in single-molecule optical trap experiments. Biophys. J. 97, 2128-2136 (2009).] In blue: example force-extension curve of the DNA construct used as a tether for the hybridization experiments. The dotted line is a polymer model of the DNA construct (see Methods). The hybridization construct data and model have been offset to lower extension (-300 nm) for clarity.

Supplementary Note – Detailed parts list for instrument

The following is a list of essential parts required to construct the instrument. Please refer to the instrument layout in **Fig. 1**.

1064-nm trapping laser, IPG Photonics YLR-5-1064-LP

532-nm fluorescence excitation laser, World Star Tech TECGL-30

Piezo mirror stage, Mad City Labs Nano-MTA2 Invar

Sample chamber stage, motors: Newport CMA-12CCCL, controller: Newport ESP300

AOM1, IntraAction ATM-803DA6B

AOM2, IntraAction AOM-802AF1

Microscope objectives, Nikon CFI Plan APO VC 60x 1.2 NA water immersion

QPD, Pacific Silicon Devices QP154-Q-TO1032

APD, PerkinElmer SPCM-AQRH-14

CCD camera, Watec WAT-902H2

frame grabber pc card, Matrix Vision mvDELTAe-BNC

Optical filters:

F1, Chroma Technology HQ545lp-laser

F2, Thorlabs FES1000

F3, Semrock NF01-532U-25

F4, Newport 10LF25-1064

Dichroic mirrors:

D1 and D2, CVI SWP-45-RU1064-TUVIS-PW-1025-C

D3, CVI SWP-45-RU532-TUVIS-PW-1025-C

D4, Semrock LPD01-532RS-25

Electronics:

AOM2 driver electronics, ME-801.5-6

Digital RF synthesizer board, Analog Devices AD9852/PCBZ

Digital RF synthesizer board power supply, Acopian A3.3NT350

Digital RF synthesizer board crystal oscillator, Conner-Winfield HTFL5FG5-049.152M

RF power amplifier, Mini-Circuits ZHL-5W-1

RF power amplifier power supply, Acopian 24PH15AM

Low noise RF cabling, Mini-Circuits CBL-25FT-SMSM+

Instrument control and data acquisition pc card, National Instruments PCIe-7852R

Programming, LabVIEW 2009